Sigma J Eng & Nat Sci 34 (2), 2016, 159-173

Sigma Journal Engineering and Natural Sciences
Sigma Mühendislik ve Fen Bilimleri Dergisi

Research Article / Araştırma Makalesi

INVESTIGATION ON ACTIVITIES OF METAL OXIDES CATALYZED AMMONIA BORANE HYDROLYSIS

Bilge COŞKUNER FİLİZ, Sabriye PİŞKİN*

Yildiz Technical University, Department of Chemical Engineering, Esenler-ISTANBUL

Received/Geliş: 16.12.2015 Accepted/Kabul: 25.04.2016

ABSTRACT

In the present study, the activities of metal oxide - catalyzed ammonia borane (NH_3BH_3, AB) hydrolysis were investigated. Two non-noble metal oxide catalysts, cobalt oxide (Co_3O_4) and copper oxide (CuO), were synthesized by sol-gel method and catalytic activity tests were performed. The comparative kinetic analyses were investigated via Power Law and Bimolecular kinetic models. Hydrogen generation rates were achieved 4381.20 ml $H_2.g^{-1}cat.min^{-1}$ and 835.04 ml $H_2.g^{-1}cat.min^{-1}$ for Co_3O_4 and CuO metal oxides catalysts, respectively. Despite the different hydrogen generation rates of metal oxides catalysts, both metal oxides had similar apparent activation energy as 46.28 $kJ.mol^{-1}$ for Co_3O_4 and 45.64 $kJ.mol^{-1}$ for CuO with free of reactant concentration behaviors. According to the bimolecular kinetic model investigations, Co_3O_4 had stronger relationship with NH_3BH_3. Co_3O_4 metal oxide catalyst was found to be more active for NH_3BH_3 hydrolysis in order to generate hydrogen gas for practical energy applications.
Keywords: Metal oxides, ammonia borane, reaction kinetic, hydrogen, hydrolysis.

1. INTRODUCTION

Boron-nitrogen-hydrogen containing compounds (BNHC) have great potential for improving hydrogen storage systems. Ammonium borane (NH_3BH_3, AB) is one of the most attractive compound among BNHC with rich hydrogen content (wt. 19.6 %) and prominent properties-stability, transportability and non-toxicity etc.- as an environmentally desirable carrier of hydrogen due to these [1-3].

The efficient hydrogen generation from an aqueous solution of AB with higher pH value than 7 could be achieved in presence of catalytic materials via hydrolysis process under ambient conditions. By changing the mole of water molecules react with AB molecules, borate anion, boric acid (H_3BO_3) or tetrahydroxyborateanion ($B(OH)_4^-$) could be formed in hydrolysis medium [4]. The three hydrolysis reactions were given below in Eq. [1], [2] and [3]:

$$NH_3BH_{3(aq)} + 2H_2O_{(l)} \rightarrow NH_4^+{}_{(aq)} + BO_2^-{}_{(aq)} + 3H_{2(g)} \quad (1)$$

* Corresponding Author/Sorumlu Yazar: e-mail/e-ileti: piskin@yildiz.edu.tr, tel: (212) 383 47 29

$$NH_3BH_{3(aq)} + 3H_2O_{(l)} \rightarrow NH_{3(aq/g)} + H_3BO_{3(aq)} + 3H_{2(g)} \quad (2)$$

$$NH_3BH_{3(aq)} + 4H_2O_{(l)} \rightarrow NH_4^+{}_{(aq)} + B(OH)_4^-{}_{(aq)} + 3H_{2(g)} \quad (3)$$

The aqueous solution of pristine AB catalytic hydrolysis were widely investigated thereness of various catalytic materials such as noble metals [5-6], non-noble metals [7-8], acids and bases [9-10], supported metals [11-12], etc. Besides noble metals catalyzed dehydrogenations were highly active, their prices increase product cost of the hydrogen generation systems. On the other hand, studies reported that with non-noble metal catalysts such as Co, Ni, Cu etc. AB undergoes dissociation and hydrolysis with a high kinetics to release H_2 with H_2/AB=3 [13-15]. The present low-cost catalyst, high hydrogen generation rate and mild reaction conditions (at room temperature in aqueous solution) represent a promising step toward the development of ammonia borane hydrolysis as a viable on-board hydrogen-storage and supply material [16].

Yan et.all. prepared an amorphous and well dispersed Co nanoparticles had been in situ synthesized in aqueous solution at room temperature and found high activation for ammonia borane hydrolysis [16]. Kadilindi et.all. studied AB hydrolysis for the generation of hydrogen by using first row transition metal ions, such as Co^{2+}, Ni^{2+}, and Cu^{2+}. They found that first row transition metal-assisted AB hydrolysis were highly catalytically active for hydrogen generation [17]. In their study of Kadilindi et. all. prepared Cu, Cu@Cu_2O core shell, and Cu_2O particles which were active catalysts for the generation of H_2 via hydrolysis of AB. They indicated that Cu@Cu_2O core shell and Cu_2O nanoparticles were more active than pure Cu nanoparticles. The catalysts showed very good recyclability and demonstration of the use of catalysts with greater stability comprising cheaper and more abundant first-row transition metals for the generation of H_2 from AB [18].

In the present study, the comparative activities and kinetics of metal oxides (Co_3O_4 and CuO) in AB hydrolysis were investigated. We focused on preparation of non-noble metal oxides preparation via sol-gel process by two different metal precursor ($Co(NO_3)_2.6H_2O$ and $Cu(NO_3)_2.6H_2O$) and the activity tests of metal oxides were performed at various hydrolysis temperatures (22°C, 40°C, 60°C, and 80 °C); as a last step the investigation of hydrolysis kinetics were done by power law and bimolecular kinetic models. In conclusion, we found that Co_3O_4 was a pretty active than CuO metal oxides for hydrogen generation from AB. Both showed similar reactant concentration free behavior with zero-order reaction kinetic model and their apparent activation energy were 46.28kJ.mol^{-1} for Co_3O_4 and 45.64kJ.mol^{-1} for CuO. According to bimolecular investigation, the adsorption interaction of AB molecules on Co_3O_4 and AB was almost four times higher than CuO-AB which explains the activity of Co_3O_4.

2. EXPERIMENTAL PART

2.1. Materials

All reagents used in this research were analytical grade. Cobalt(II)nitrate hexahydrate ($Co(NO_3)_2.6H_2O$, %97) and, cupper(II)nitrate hexahydrate ($Cu(NO_3)_2.6H_2O$, %97), from Merck, citric acid ($C_6H_8O_7$, %99.5) from Carlo Erba, and ammonia borane (NH_3BH_3, %97) from Aldrich were used as received.

2.2. Sol-gel Synthesis and Characterization Non-Noble Metal Oxides

The non-noble metal oxide catalysts were synthesized by sol-gel method. As a first step of preparation, 0.25 M $C_6H_8O_7$ solution was prepared at 80°C and nitrate precious ($M.(NO_3)_2$:$C_6H_8O_7$ = 0.2) was added into the aqueous solution and mixed with magnetic stirring for 2 hours and then gel structure was maintained. The remaining water molecules were removed

via drying at approximately 100°C under the vacuum condition for overnight. The dried metal oxide gel was calcined at 450°C for 4 hour to remove organic components from the structure in order to determine formation of the crystalline structure transition. Crystalline, chemical and morphology structure of obtained metal oxide catalysts were performed by using XRD (Panalytical X'Pert-Pro diffractometer with CuKα radiation (λ = 0.15418 nm)), FT-IR (Perkin Elmer Spectrum One) and SEM (a JEOL JSM 5410 LV) analysis techniques. In addition to this, the specific surface area was measured by N_2 adsorption Brunauer-Emmett-Teller (Quantachrome) technique.

2.3. Activity Tests of Metal Oxides in AB Hydrolysis

The activity tests of metal oxides in AB hydrolysis were performed in hydrolysis system which has 15 ml hydrolysis - glass reactor capacity with magnetic stirrer (750 rpm). The hydrogen generation from 0.12 M AB solutions in presence of metal oxide catalysts (0.005 g) were performed at constant hydrolysis temperature (22°C-80°C) which was checked by temperature control system. The generated hydrogen was measured by water displaced method which was easily converted into the conversion of AB and plotted against the reaction time.

3. KINETICS OF METAL OXIDES IN AB HYDROLYSIS

Reaction behavior of catalytic hydrogen generation from aqueous AB in presence of metal oxide catalysts were analyzed by using of kinetic modelling. The generated hydrogen was converted into AB-reactant. Power law models (zero-order, first-order, and second- order reaction) and bimolecular kinetic models (Langmuir-Hinshelwood and Micheal-Menten) were applied to decide the reaction behavior of the catalytic hydrogen generation from aqueous AB [19-24].

3.1. Power Law Models

The power law models express the rate of the reaction as a function of the concentration of the reactants involved in the reaction. The power law kinetic models of metal oxides in AB hydrolysis were investigated by preference of zero, first and, second order kinetics.

$$\frac{dC_{AB}}{dt} = -r_{AB}.C_{AB}^{n} = -k(T).C_{AB}^{n} \quad (3)$$

C_{AB} was the concentration of AB, r was the rate of react ion, k was the reaction rate constant base on temperature. After determining of the reaction order a plot of Arrhenius law's slope gave activation energy of AB catalytic hydrolyses and also its intercept was Arrhenius constant. The zero-order kinetic model has been shown in systems which was independent of any reactant concentration (n=0) (Eq.4).

$$(C_{AB0} - C_{AB}) = -k(T).t \quad (4)$$

The first-order kinetic(n=1) was model-integrated form- as seen Eq.5 which depended on the concentration of reactant:

$$\ln\left(\frac{C_{AB0}}{C_{AB}}\right) = k(T).t \quad (5)$$

The second-order kinetic (n=2) could be expressed the concentrations of one second order reactant:

$$\left(\frac{1}{C_{AB}} - \frac{1}{C_{AB0}}\right) = -k(T).t \quad (6)$$

3.2. Bimolecular Kinetic Models

The catalytic hydrogen generations from aqueous AB in presence of non-noble metal oxide catalysts were captured by bimolecular kinetic models that are presented below. Investigation of reaction mechanism gave ideas about interaction between active catalysts sides and reactant molecules and the formation way of target molecules. Despite the power law models, bimolecular kinetic models gave further information of molecular interactions [19-24].

3.2.1. Langmuir-Hinshelwood Model

Langmuir-Hinshelwood model was the most common kinetic for explaining the heterogeneous catalysts mechanism. In heterogeneous phase reactions, interaction between catalysts and reactant had two steps according to this model. The reactant firstly, adsorbed on the surface of the catalysts and then as a second step reaction occurred on adsorbed species to generate hydrogen. Hydrogen generation rate could be expressed as below:

$$\frac{dC_{AB}}{dt} = -r_{AB} = -k\ \frac{K_a C_{AB}}{1+ K_a C_{AB}} \tag{7}$$

K_a, C, and k represented the adsorption constant, concentration, and reaction rate respectively. Calculation of K_a (Eq.8) was fulfilled by minimizing of correlation coefficients of data maintained at 40°C and 60°C.

$$min_{K_a} f(K_a) = \left(1 - R^2_{40°C}\right) + \left(1 - R^2_{60°C}\right) \tag{8}$$

Reaction rate according to this model could be determined by usage of integrated formula of Eq.9:

$$\frac{1}{K_a} \ln\left(\frac{C_{AB_o}}{C_{AB}}\right) + \left(C_{AB_o} - C_{AB}\right) = k.t \tag{9}$$

3.2.2. Michaels–Menten Model

Heterogeneous catalysis mechanism has some problems with characterization of active sites as same as biocatalysts. Metal oxide catalyst shared almost same challenges with biocatalysts, where and which active sites they have for reaction. Due to the same problems in heterogeneous catalysts and biocatalysts, we wanted to apply Michaels-Menten reaction mechanism for investigation of catalytic hydrogen generation from aqueous AB in presence of non-noble metal oxide catalysts. The main steps of this kinetic adsorption were reactant on catalyst and surface reaction for hydrogen generation.

This bimolecular approach could be formulized as given below:

$$\frac{dC_{H_2}}{dt} = \frac{\vartheta_{max} C_{AB}}{K_M + C_{AB}} \tag{10}$$

ϑ_{max} values defined as maximum H_2 generation rate in logarithmic phase of hydrolysis reaction and K_M was Micheal-Mentencontstant. In this method, Lineweaver–Burk plot made easier for determination of these values and the Eq. [11] became as below:

$$\frac{1}{\frac{dC_{H_2}}{dt}} = \frac{K_M}{\vartheta_{max}} . \frac{1}{C_{AB}} + \frac{1}{\vartheta_{max}} \tag{11}$$

4. RESULTS AND DISCUSSION

4.1. Characterization Non-Noble Metal Oxides

In this study, non-noble metal oxides were synthesized according to the sol-gel procedures. After heat treatment at 100°C metal cobalt, and copper nitrates reacted with alkoxide; pink, and

blue gels were obtained, respectively. All colorful powders converted into black solid after calcination process at 450°C for 4 hours.

Figure 1. represents the XRD patterns of non-noble metal oxides. According to the XRD analysis, both non-noble metal oxides were formed in one phase metal oxide successfully and the structure did not contain oligomer, metal precursors. Cobalt oxide catalysts had a cubic crystalline structure, while copper oxide catalyst had monoclinic structure. Cobalt oxide catalyst was Co_3O_4 form with 03-065-3103 JCPDS number and, copper oxide catalyst was CuO form with 00-005-0661 JCPDS number. Characteristic peaks of Co_3O_4 were observed for the diffraction angles of 31.38^0, 36.98^0 and, 65.49^0 with (2 2 0), (3 1 1) and, (4 4 0) reflection lines, respectively.The XRD analyses of the obtained CuO catalyst-calcinated at 450ºC- indicate that the 35.66^0, 38.85^0 and 48.95^0 (-1 1 1), (1 1 1) and (-2 0 2) were present in the standard patterns in the current powder diffraction file database. Crystalline sizes of catalysts were calculated based on Scherrer equation. Beside catalysts were prepared under same conditions, CuO catalyst (49.92 µm) had almost twice time bigger crystalline size than Co_3O_4 catalyst (20.32 µm). The BET results show that Co_3O_4 catalyst had far larger surface area and pore volume (18.67 $m^2.g^{-1}$ and 0.1666 $cm^3.g^{-1}$) compared to CuO catalyst (0.44 $m^2.g^{-1}$ and 00041 $cm^3.g^{-1}$), besides their pore sizes almost same. In addition to these results, the SEM images (with 1000 magnification) of non-noble metal oxides shows that both catalysts had a similar particle shape with a similar average particle size and wide range particle size distribution (Figure 2.).

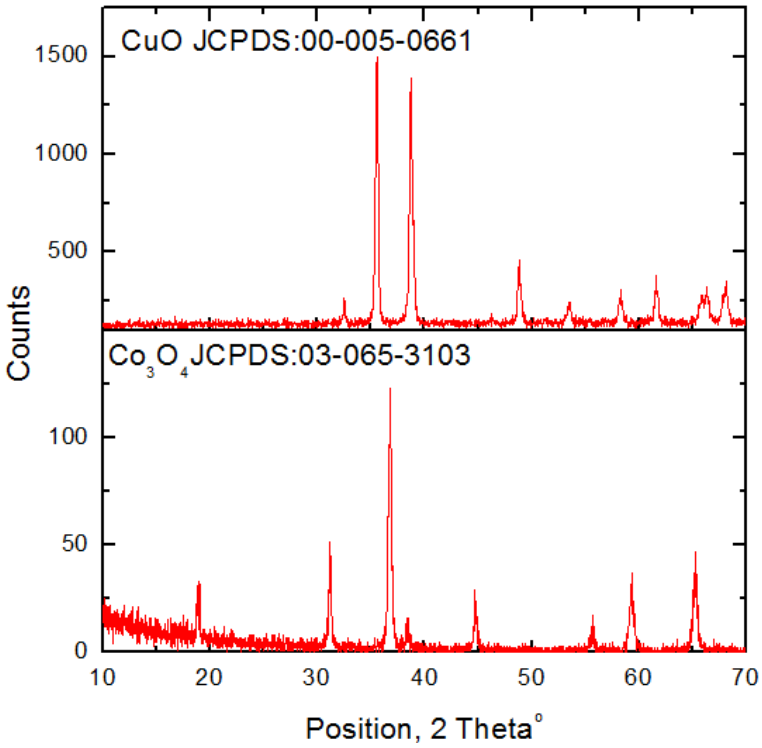

Figure 1. XRD Diagrams of non-noble metal oxide catalysts

Figure 3. shows the FT-IR spectrum of non-noble metal oxides catalysts and organic ligand. The infrared absorption spectrum of citric acid exhibits infrared absorption bands related to the

presence of C=O stretching (1760-1670 cm^{-1}), C-O stretching (1260-1000 cm^{-1}) and O-H bending (1440-1400 cm^{-1}) [24]. As it could be clearly seen from spectrum, we did not observed any organic elements bonding which organic ligands had between 650-2000 cm^{-1} range in non-noble metal oxides catalysts analysis results. This means that all organic compounds were removed from catalyst structure after calcination process.

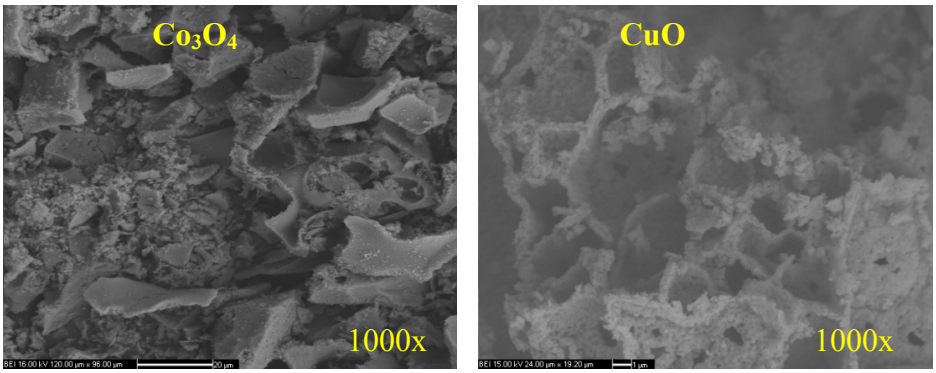

(a) (b)

Figure 2. SEM images of non-noble metal oxide catalysts at 1000 magnification

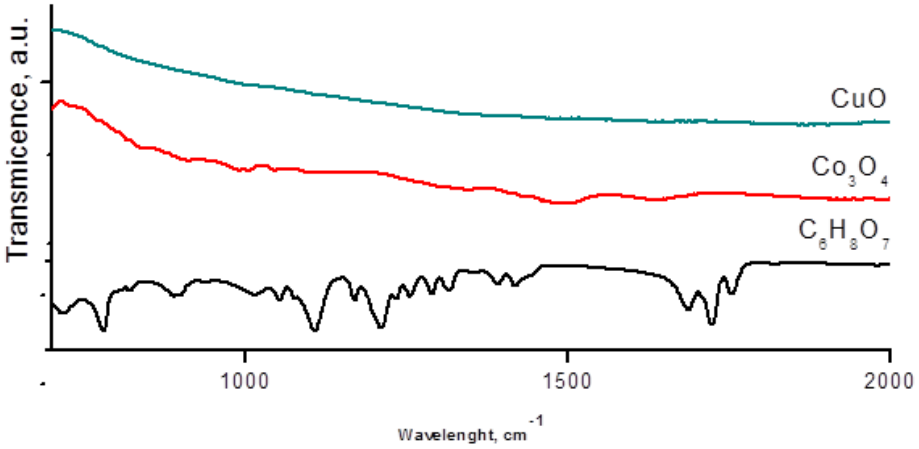

Figure 3. FT-IR spectrums of non-noble metal oxide catalysts and organic precursor

4.2. Catalytic Hydrogen Generation from Aqueous AB

The catalytic hydrogen generations from aqueous AB in presence of metal oxide catalysts were performed at variety of reaction temperatures (22°C-80°C). All non-noble metal oxides shows different catalytic hydrogen generation tendency. Co_3O_4 and CuO catalysts were active for this reaction, they showed several induction time also based on reaction temperature []. The catalytic hydrogen generation data was applied linear regression and converted into conversion of H_2, also 100 % hydrogen generation were obtained from aqueous AB solution in presence of Co_3O_4 and CuO catalysts at all temperatures (Figure 4.).

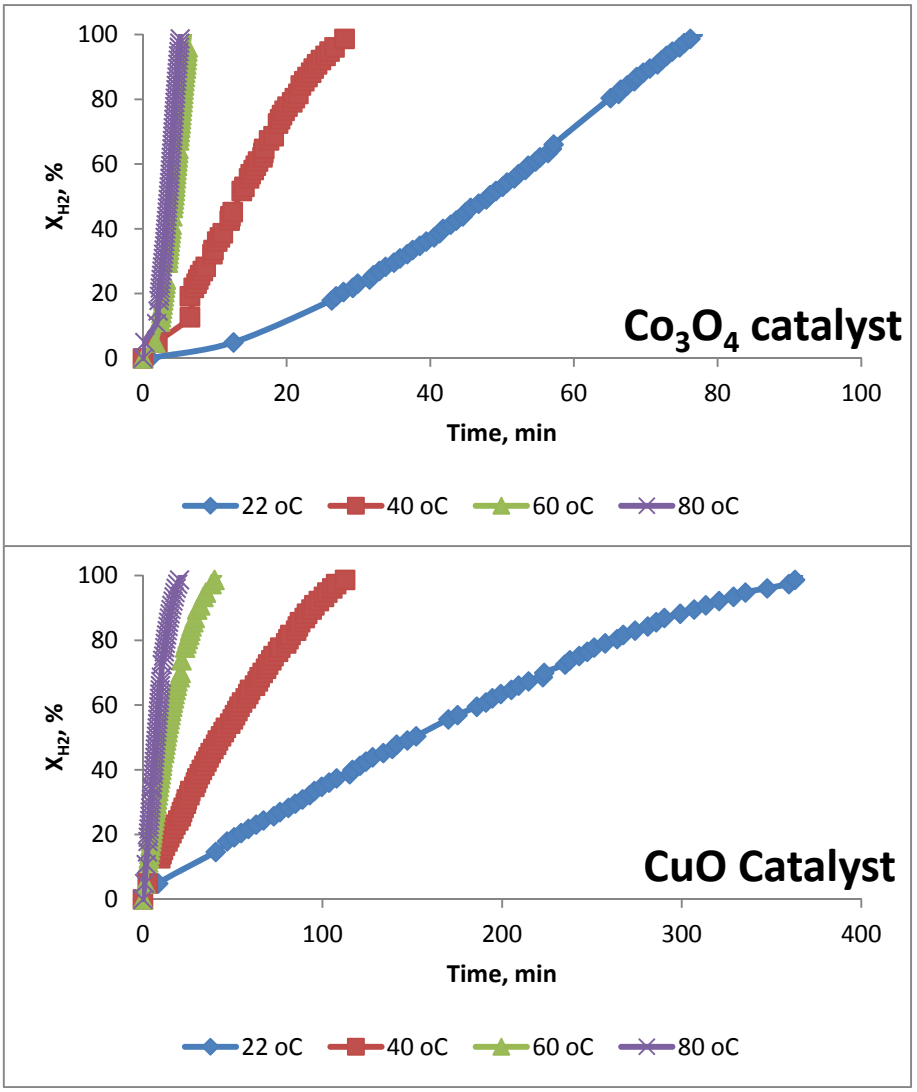

Figure 4. H_2 generation yield at different temperatures for Co_3O_4 and CuO catalysts

Among the metal oxide catalysts tested, Co_3O_4 catalyst exhibited maximum enhancement in the rate of catalytic hydrogen generation. While CuO had 835.04 $mlH_2.g^{-1}cat.min^{-1}$ hydrogen generation rate, Co_3O_4 catalyst was almost 525% faster with 4381.20 $mlH_2.g^{-1}cat.min^{-1}$ hydrogen generation rate at 80°C (Table 2). The increase in the rate of reaction was found to be proportional to the temperature. Just as temperature increased from 22°C to 80°C, reaction rate were increased from 41.66 $mlH_2.g^{-1}cat.min^{-1}$ to 835.04 $mlH_2.g^{-1}cat.min^{-1}$ with 2000 % in presence of CuO catalysts. This inclination was same and 1719 % increment obtained in hydrogen generation rate while reaction catalyzed by Co_3O_4 catalyst. It could be noted that the enhancement in the reaction rate in the presence of Co_3O_4 catalyst was significant in all cases compared to that for the CuO catalyzed reaction rate.

Table 1. Hydrogen Generation Rate and Power law reaction model parameters of non-noble metal oxide catalysts

Metal oxide catalysts	Hydrogen Generation Rate, ml $H_2.g^{-1}cat.min^{-1}$				Power law model					
					Zero-order		First-order		Second-order	
	22, ^{0}C	40, ^{0}C	60, ^{0}C	80, ^{0}C	E_a ,kJ.mol^{-1}	k_0	E_a, kJ.mol^{-1}	k_0	E_a, kJ.mol^{-1}	k_0
Co_3O_4	254.92	621.85	3556.20	4381.20	46.28	12.57	44.55	14.86	44.10	17.70
CuO	41.66	134.86	423.46	835.04	45.64	10.53	46.14	13.64	47.32	17.10

4.3. Kinetic Modelling

Nowadays, kinetic modelling of catalyzed hydrogen generation systems are essential due to they ensure required knowledge related with the role of the reactants and the catalyst behavior. This knowledge will be significant to design on board or mobile reactors for hydrogen systems.
For kinetic modeling, the hydrogen generation rate was converted to AB concentration as function of time. The kinetic data was analyzed in terms of power law and bimolecular kinetic models to determine the reaction kinetics; activation energy of the reaction was then calculated based on Arrhenius kinetic assumption.

4.3.1. Power Law Models

Zero-order, first-order and, second-order power law models were used to describe the kinetic behavior of the catalytic hydrogen generation from aqueous AB in presence of metal oxide catalysts. The catalyzed AB consumption to generate hydrogen as a concentration was analyzed according to the zero-order, first-order and, second order power law models graphed as a function of time (Figure 5. and 6.).

Figure 5. shows the zero-order (A), first-order (B) and, second-order (C) reaction kinetic model curves and Arrhenius kinetic assumption at 22°C-80°C for Co_3O_4 catalyzed hydrogen generation in selected range. The power law kinetic model calculations data were plotted versus time. The correlation co-factor values were determined by linear regression calculations. According to these results correlation coefficient of zero-order kinetic models was found that the best fitted for Co_3O catalyst. This means that hydrolysis of AB in the presence of Co_3O_4 catalyst was independent of AB concentration. The plot of Arrhenius kinetic assumption was plotted hydrogen generation rate versus 1/T for calculation of kinetic parameters of catalytic hydrogen generation from aqueous AB in presence of Co_3O_4 catalysts. The Arrhenius graphs of power law models were given as inserted in Figure.5 A, B and, C. The slope and y-intercept of Arrhenius graphs inset of Figure 5. were used to calculate apparent activation energy and Arrhenius constant, respectively. The all kinetic parameters were given in Table 2. The activation energy and Arrhenius constant of catalytic hydrogen generation from aqueous AB in presence of Co_3O_4 catalyst were determined as 46.28 kj.mol^{-1} and 12.57min^{-1}, respectively.

Figure 6. shows power law kinetic models and Arrhenius graphs of hydrogen generation in presence of CuO catalysts at 22°C-80°C range. The same procedures were applied to data set with Co_3O_4 catalyst. Depending on correlation co-factors given in Figure.6 (A), (B) and, (C), we can say that at higher reaction temperatures as 60°C-80°C reaction tended to be more AB concentration depends, while it was independent of AB concentration at lower temperature as 22°C-40°C. The apparent activation energy value was calculated as 45.64 kj.mol^{-1}. As we know apparent activation energy is a minimum energy requirement that must be met for a chemical reaction to occur. Besides these values almost same for Co_3O_4 and CuO catalysts, the hydrogen generation rates were motley.

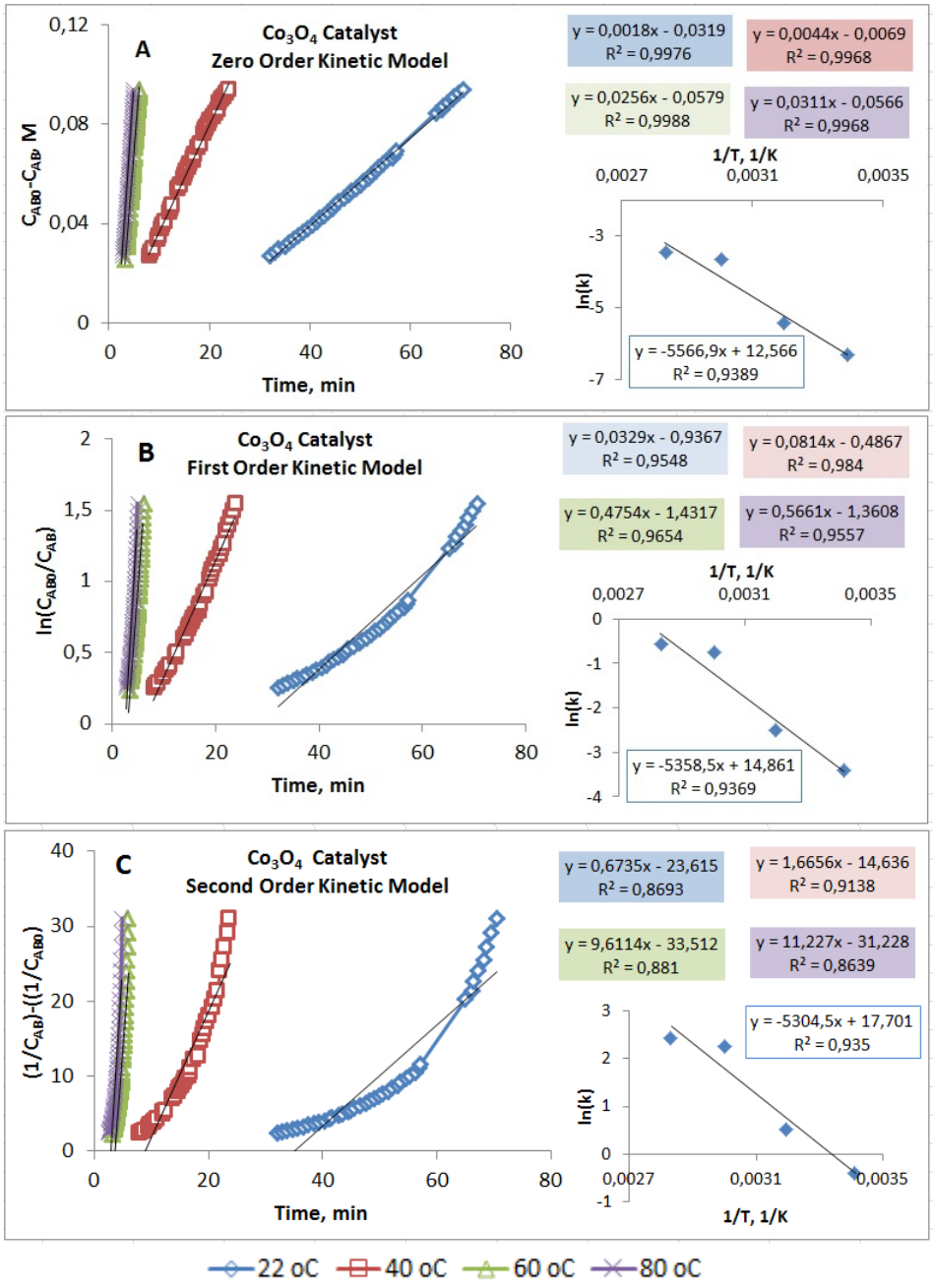

Figure 5. Power law models for Co_3O_4 catalyst

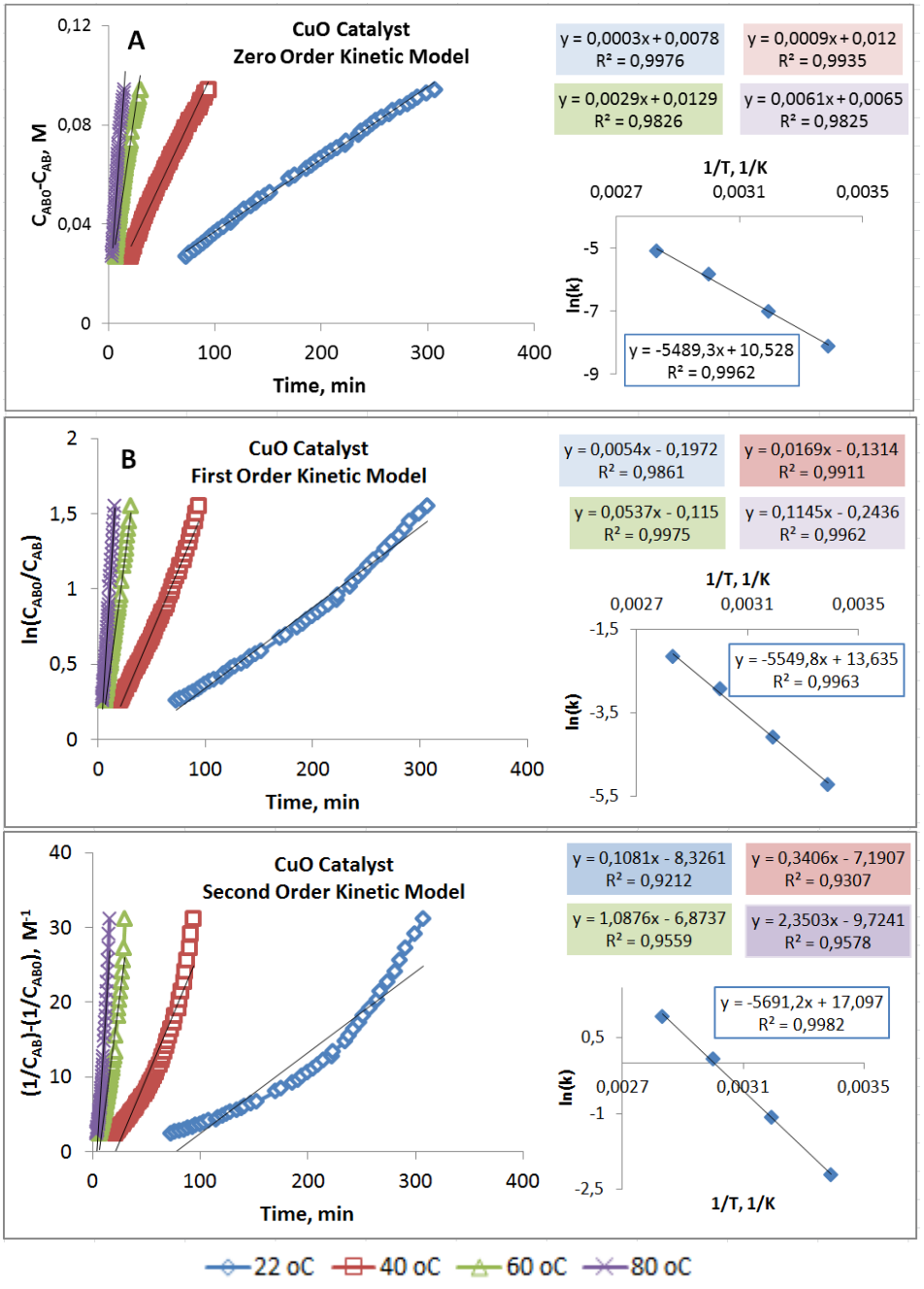

Figure 6. Power law models for CuO catalyst

4.3.2. Bimolecular Kinetic Models

Figure 7. presents the Langmuir-Hinshelwood investigation of active Co_3O_4 and CuO catalysts. Accordingly, the Langmuir-Hinshelwood reactant firstly adsorbs on the surface of the catalyst and then as a second step reaction occurs on the adsorbed species to generate hydrogen [21, 23]. As a first step of this model adsorption constant K_a was calculated based on Eq. 8 and graphs were given in Figure.7a. Then, the model applied via Eq. 9 to investigate mechanism (Figure.7b) and Arrhenius assumption graphs were given in Figure.7c. Co_3O_4 and CuO catalysts had considerably different K_a values with 108 $L.mol^{-1}$ and 28 $L.mol^{-1}$, respectively. In the Langmuir model, K_a represented the affinity between the catalyst and the reactants. This means that Co_3O_4 catalyst had more affinity than CuO catalyst with AB. For all that apparent activation energy values of both catalysts were almost similar, 45.80 $kJ.mol^{-1}$ for Co_3O_4 catalyst and 44.23 $kJ.mol^{-1}$ for CuO catalyst (Table 2.). Attraction between catalysts and AB were divergent and, the energy for starting the reaction was same. It was directed attention that completion periods and K_a values of catalysts were significantly different. The adsorption on the surface of the CuO catalyst was low so the reaction occurred slower than Co_3O_4 catalyst.

Figure 8. shows the Michaelis-Menten kinetic model and Arrhenius kinetic assumption graphs of both catalysts. Michaelis-Menten kinetic model hypothesizes reversible adsorption on the active sites and the main steps of the kinetic adsorption of reactant on catalyst surface [21,23]. The logarithmic phase of hydrolysis reaction were determined according to the instant reaction rate and its linearity. The Lineweaver-Burk plots were given in Figure.8a and b, which calculated based on Eq. 9 and 10. ϑ_{max} and K_M values were given in Table 2. These two kinetic values had direct proportion with temperature in both catalytic systems. In presence of Co_3O_4 and CuO, by increasing the temperature from 22^{0}C to 80^{0}C, ϑ_{max} increased ~31 % and ~81 %, respectively. Temperature did not effect on ϑ_{max} values of Co_3O_4 significantly. The affinity of reactant and catalyst was determined via Michaels constant K_M. The catalyst, reactant, reaction conditions effects this value. As seeing from Table 2, K_M values were different for catalysts. While the temperature increased, K_M values did not change dramatically which means the temperature did not improve catalytic efficiency. Small values of K_M mean more efficient catalysts in which it also depended on the reactant and reaction conditions as it could be seen from results. According to the Langmuir Hinshelwood, the k value mean the total number of adsorption sites on the surface of the catalyst now appeared explicitly as the reaction rate value for this elementary adsorption step (Table 2). Moreover, accordingly to Michaelis-Menten kinetic model, the Co_3O_4 had higher ϑ_{max} value than the AB solution as E_a was lower than it (Table 2).

Table 2. Bimolecular reaction model parameters of non-noble metal oxide catalysts

Kinetic Model	Kinetic parameters		Metal oxide catalysts	
			Co_3O_4	CuO
Langmuir Hinshelwood	K_0,$L.mol^{-1}$		108	28
	E_a, $kJ.mol^{-1}$		45.80	44.23
	k_0		12.51	10.48
Micheal-Menten	ϑ_{max}	22,^{0}C	0.018	0.001
		40,^{0}C	0.051	0.006
		60,^{0}C	0.161	0.025
		80,^{0}C	0.214	0.057
	K_M	22,^{0}C	0.186	0.032
		40, ^{0}C	0.059	0.037
		60,^{0}C	0.071	0.110
		80,^{0}C	0.005	0.153
	E_a, $kJ.mol^{-1}$		38.72	57.47
	k_0		11.87	16.89

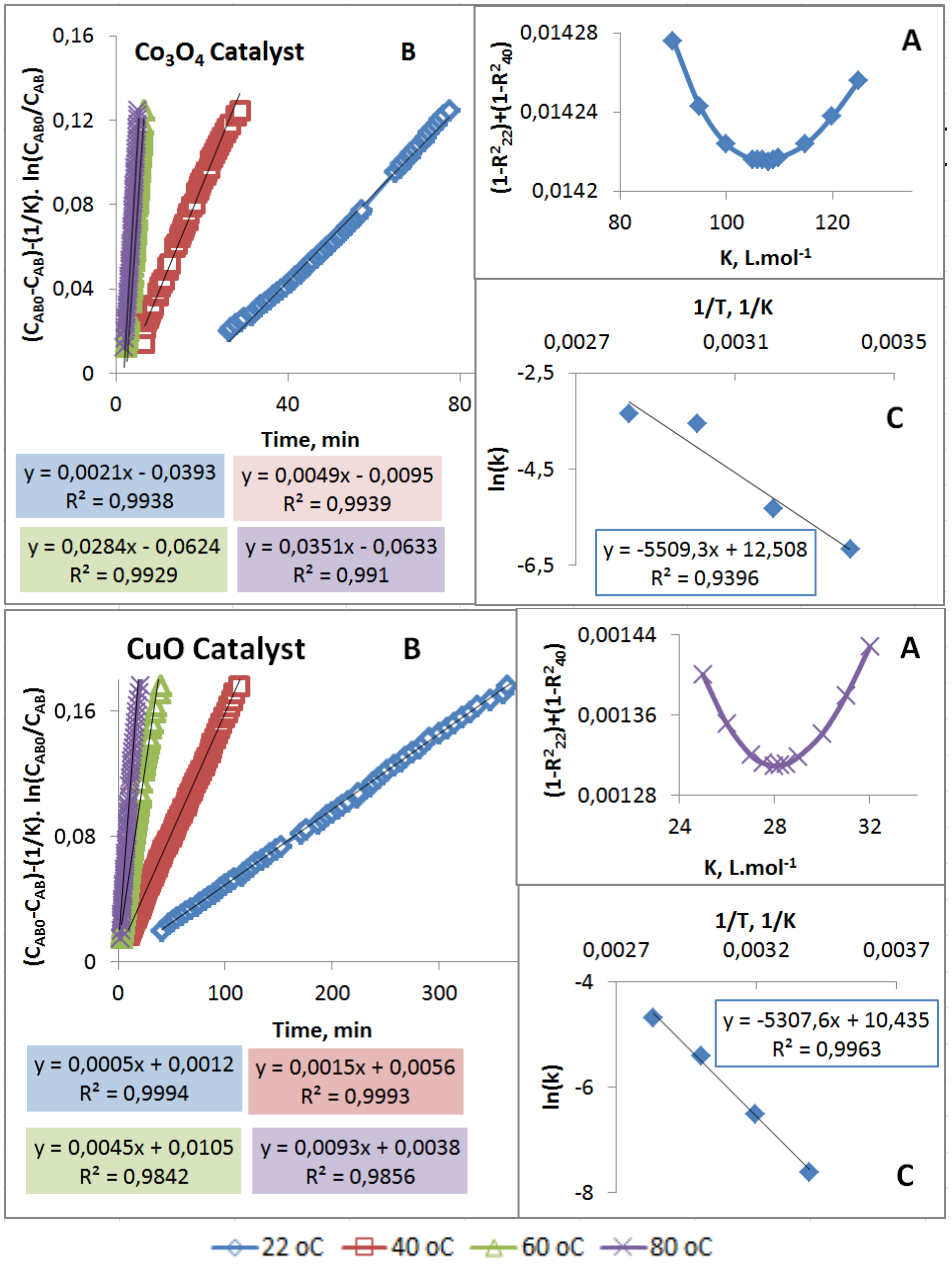

Figure 7. Langmuir kinetic model for Co_3O_4 and CuO catalysts

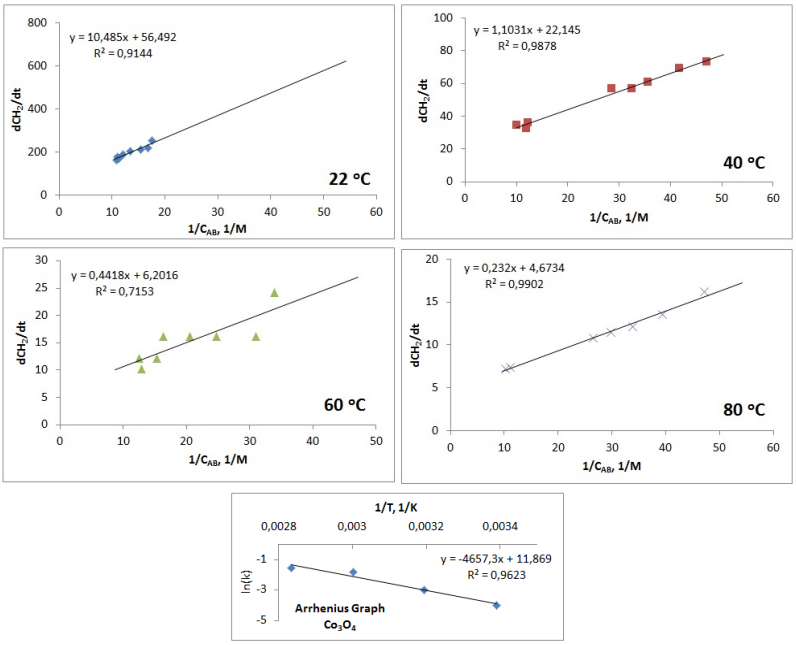

(a)

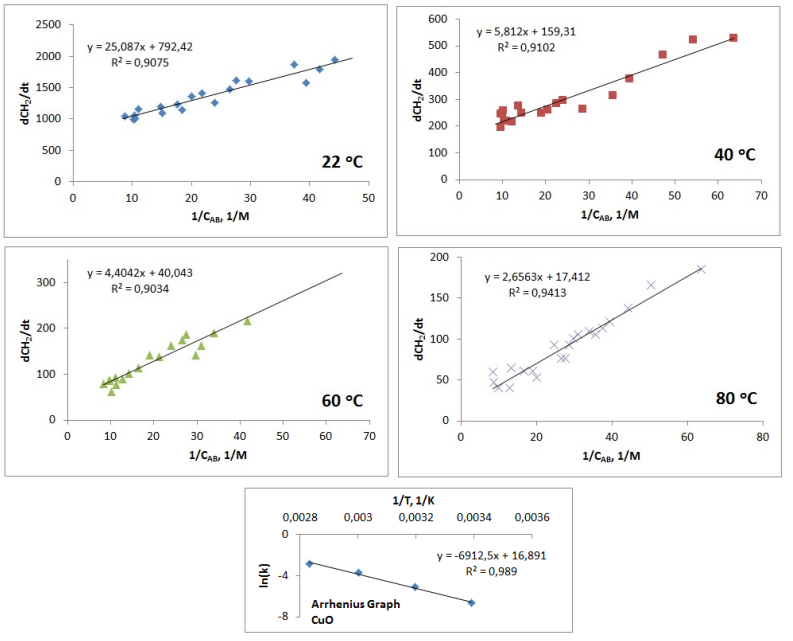

(b)

Figure 8. Michealis-Menten kinetic model for (a) Co_3O_4 and (b) CuO catalysts and,(c) Arrhenius plot

4. CONCLUSION

In the present study, the comparative activities and kinetics of metal oxides (Co_3O_4 and CuO) in AB hydrolysis were investigated. The kinetic studies showed that Co_3O_4 had significantly activation for AB hydrolysis. Both metal oxides activations were free of AB concentration as a zero-order reaction kinetic model with similar apparent activation energy 46.28 $kJ.mol^{-1}$ for Co_3O_4 and 45.64 $kJ.mol^{-1}$ for CuO. According to bimolecular kinetic investigation, the adsorption interaction of AB molecules on Co_3O_4 and AB is almost four times higher than CuO-AB which explains the activity of Co_3O_4.

Acknowledgments / Teşekkür

The authors also would like to thank the Yildiz Technical University Research Foundation (Project no: 2015-07-01-DOP01) for its financial support.

REFERENCES / KAYNAKLAR

[1] Ramachandran, P. V.,Mistry, H., Kulkarni, A. S., &Gagare, P. D. (2014) Ammonia-mediated, large-scalesynthesis of ammoniaborane. DaltonTransactions, 43:44:16580-16583.

[2] Jiang, Hai-Long, and Qiang Xu. (2011) "Catalytic hydrolysis of ammonia borane for chemical hydrogen storage" Catalysis Today 170: 1: 56-63.

[3] Yoon, Chang Won, and Larry G. Sneddon. (2006) Ammonia triborane: a promising new candidate for amineborane-based chemical hydrogen storage. Journal of the American Chemical Society 128: 43:13992-13993.

[4] Moussa, G.,Moury, R., Demirci, U. B., &Miele, P. (2013) Borates in hydrolysis of ammoniaborane. İnternational Journal of Hydrogen Energy, 38:19: 7888-7895.

[5] Xi, Pinxian, Fengjuan Chen, Guoqiang Xie, Cai Ma, Hongyan Liu, Changwei Shao, Jun Wang, Zhihong Xu, Ximing Xu, and Zhengzhi Zeng. (2012) Surfactant free RGO/Pd nanocomposites as highly active heterogeneous catalysts for the hydrolytic dehydrogenation of ammonia borane for chemical hydrogen storage. Nanoscale 4:185597-5601.

[6] Cao, Nan, Wei Luo, and Gongzhen Cheng. (2013) One-step synthesis of graphene supported Ru nanoparticles as efficient catalysts for hydrolytic dehydrogenation of ammonia borane. International Journal of Hydrogen Energy 38: 27: 11964-11972.

[7] Barakat, Nasser AM. (2013) Effective Co–Mn–O nanofibers for ammonia borane hydrolysis. Materials Letters 106: 229-232.

[8] Wang, Hong-Li, Jun-Min Yan, Zhi-Li Wang, and Qing Jiang. "One-step synthesis of Cu@ FeNi core–shell nanoparticles: Highly active catalyst for hydrolytic dehydrogenation of ammonia borane". International journal of hydrogen energy 37, no. 13 (2012): 10229-10235.

[9] Kelly, Henry C., and Vic B. Marriott. (1979) Reexamination of the mechanism of acid-catalyzed amine-borane hydrolysis. The hydrolysis of ammonia-borane. Inorganic Chemistry 18:10: 2875-2878.

[10] Chandra, Manish, and Qiang Xu. (2006) Dissociation and hydrolysis of ammonia-borane with solid acids and carbon dioxide: an efficient hydrogen generation system. Journal of Power Sources 159: 2: 855-860.

[11] Rachiero, Giovanni P., Umit B. Demirci, and Philippe Miele. (2011) Bimetallic RuCo and RuCu catalysts supported on γ-Al 2 O 3. A comparative study of their activity in hydrolysis of ammonia-borane. International Journal of Hydrogen Energy 36:12: 7051-7065.

[12] Liang, Hongyan, Guozhu Chen, Stefano Desinan, Renzo Rosei, Federico Rosei, and Dongling Ma. (2012) In situ facile synthesis of ruthenium nanocluster catalyst supported on carbon black for hydrogen generation from the hydrolysis of ammonia-borane. International Journal of Hydrogen Energy 37: 23: 17921-17927.

[13] Wang, Hong-Li, Jun-Min Yan, Zhi-Li Wang, and Qing Jiang. (2012) One-step synthesis of Cu@ FeNi core–shell nanoparticles: Highly active catalyst for hydrolytic dehydrogenation of ammonia borane. International Journal of Hydrogen Energy 37:13: 10229-10235.

[14] Li, Pei-Zhou, Arshad Aijaz, and Qiang Xu. (2012) Highly Dispersed Surfactant-Free Nickel Nanoparticles and Their Remarkable Catalytic Activity in the Hydrolysis of Ammonia Borane for Hydrogen Generation. Angewandte Chemie International Edition 51: 27: 6753-6756.

[15] Du, Jing, Fangyi Cheng, Meng Si, Jing Liang, Zhanliang Tao, and Jun Chen. (2013) Nanoporous Ni-based catalysts for hydrogen generation from hydrolysis of ammonia borane. International Journal of Hydrogen Energy 38:14: 5768-5774.

[16] Yan, Jun-Min, Xin-Bo Zhang, Hiroshi Shioyama, and Qiang Xu. (2010) Room temperature hydrolytic dehydrogenation of ammonia borane catalyzed by Co nanoparticles. Journal of Power Sources 195: 4: 1091-1094.

[17] Kalidindi, Suresh Babu, M. Indirani, and Balaji R. Jagirdar. (2008) First row transition metal ion-assisted ammonia− borane hydrolysis for hydrogen generation. Organic Chemistry 47:16: 7424-7429.

[18] Kalidindi, Suresh Babu, Udishnu Sanyal, and Balaji R. Jagirdar. (2008) Nanostructured Cu and Cu@Cu_2O core shell catalysts for hydrogen generation from ammonia–borane. Physical Chemistry Chemical Physics 10:38: 5870-5874.

[19] Wu Z, Mao X, Zi Q, Zhang R, Dou T, Yip ACK. (2014) Mechanism and kinetics of sodium borohydride hydrolysis over crystalline nickel and nickel boride and amorphous nickel-boron nanoparticles. Journal of Power Sources.268:596-603.

[20] Basu S, Brockman A, Gagare P, Zheng Y, Ramachandran PV, Delgass WN, Gore JP (2009) Chemical kinetics of Ru-catalyzed ammonia borane hydrolysis. Journal of Power Sources. 188:238-43.

[21] Demirci UB, Miele P. (2014) Reaction mechanisms of the hydrolysis of sodium borohydride: A discussion focusing on cobalt-based catalysts. Comptes Rendus Chimie.17:707-16.

[22] Levenspiel O. Chemical reaction engineering: Wiley New York etc.; 1972.

[23] Fogler HS. Elements of chemical reaction engineering. 1999.

[24] Ozerova AM, Simagina VI, Komova OV, Netskina OV, Odegova GV, Bulavchenko OA, Rudina NA (2012) Cobalt borate catalysts for hydrogen production via hydrolysis of sodium borohydride. Journal of Alloys and Compounds.513:266-72.